Two-dimensional-Raman-terahertz spectroscopy of water: Theory

Peter Hamm and Janne Savolainen

Additional information on J. Chem. Phys.
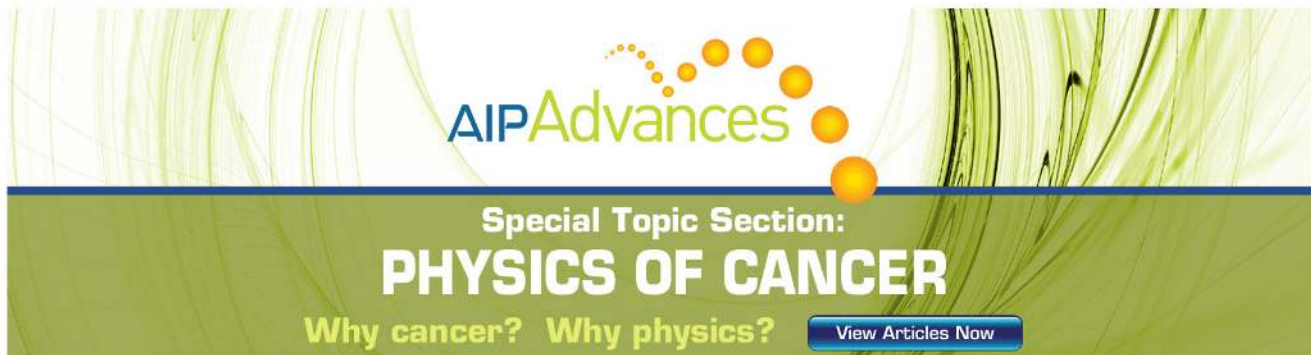
Two-dimensional-Raman-terahertz spectroscopy of water: Theory

Peter Hamm[a)] and Janne Savolainen

Physikalisch-Chemisches Institut, Universität Zürich, Winterthurerstrasse 190, CH-8057 Zürich, Switzerland

We discuss the hybrid 2D-Raman-THz spectroscopy of liquid water. This two-dimensional spectroscopy is designed to directly work in the low-frequency range of the intermolecular degrees of freedom. The information content of 2D-Raman-THz spectroscopy is similar to 2D-Raman or 2D-THz spectroscopy, but its experimental implementation should be easier. That is, 2D-Raman-THz spectroscopy is a 3rd-order nonlinear spectroscopy and as such completely avoids cascading of consecutive 3rd-order signals, which turned out to be a major difficulty in 5th-order 2D-Raman spectroscopy. On the other hand, it does not require any intense THz pump-pulse, the lack of which limits 2D-THz spectroscopy to the study of semiconductor quantum wells as the currently available pulse energies are too low for molecular systems. In close analogy to 2D-Raman spectroscopy, the 2D-Raman-THz response of liquid water is simulated from an all-atom molecular dynamics simulation, and the expected spectral features are discussed. © *2012 American Institute of Physics*. [http://dx.doi.org/10.1063/1.3691601]

I. INTRODUCTION

Water is a complex liquid due to the fast dynamics of the hydrogen-bond network that is responsible for its peculiar properties. The dynamics of bulk water has been studied extensively using 2D-IR and 3D-IR spectroscopy.[1–6] These studies concentrate on the OH- or OD-stretch vibration of water and make use of the fact that its vibrational frequency is a relatively sensitive probe of the strength of hydrogen bonding of a given OH group to its environment.[7–10] As such, the OH stretch vibration serves as local probe used to interrogate the intermolecular degrees of freedom of water. In fact, one can think of the time-dependence of a 2D-IR spectrum as the Fourier transformation of the spectral density of the intermolecular modes that couple to the OH stretch vibration.[11]

The low frequency spectrum of water, on the other hand, reports on its thermally excited intermolecular degrees of freedom in a much more direct manner. Both Raman[12–16] and THz[13,17] spectroscopy in this low frequency range have been used extensively to study pure water as well as water with various solutes. For example, if two hydrogen bonded water molecules vibrate against each other, a charge flow occurs across the hydrogen bond that ultimately leads to a vibrating dipole that can be observed in the THz spectrum as a broadband at ≈ 200 cm^{-1}.[18–21] The other to some extent distinct features in the intermolecular spectrum of water are a broadband at ≈ 600 cm^{-1}, which is commonly assigned as hindered rotations (librations) and one at ≈ 60 cm^{-1}, which is often referred to as hydrogen bond bending mode.

However, the broadening mechanism of these bands, i.e., whether they are homogeneously or inhomogeneously broadened, and the couplings between them cannot be inferred from 1D spectroscopy. Loring and Mukamel showed that this also holds for Raman spectroscopy, even though it is nonlinear in a power expansion with respect to the laser electrical fields.[22] A 2D spectrum directly in this frequency range is desirable in order to resolve the lineshape functions of these modes. 2D-Raman spectroscopy has been proposed in a seminal paper by Tanimura and Mukamel,[23] which triggered a lot of attention both theoretically[24–34] and experimentally.[35–41] It, however, turned out to be a very difficult experiment since the 5th-order Raman signal is contaminated by cascaded 3rd-order signals.[36] The experiment became feasible for certain liquids such as CS$_2$ or formamide,[37–41] but has not yet been achieved in water because of its weak Raman cross section. The 2D-THz spectroscopy, on the other hand, has recently been introduced by Elsaesser and co-workers,[42–44] but is currently limited to the study of semiconductor quantum wells due to the available low THz pulse energies. Here, we concentrate on a hybrid 2D-Raman-THz technique that has similar information content but circumvents the aforementioned problems. The pulse sequence has originally been proposed by Cho.[45]

Figure 1 compares the three techniques. In each case, two experimentally controllable times t_1 and t_2 are introduced. At time 0, the first laser pulse perturbs the system and excites a coherence of a mode of the molecular system. After time t_1, the second laser pulse interrogates the molecular system again and switches it into another coherence, much like in a correlation spectroscopy (COSY) experiment in NMR.[46] The coherence is finally read out at time $t_1 + t_2$. It is this switching between coherences which ultimately allows one to measure couplings and correlations between the various degrees of freedom of the system under study. The various spectroscopic methods shown in Fig. 1 differ by the mechanism that excites or switches coherences, i.e., whether it is done by a Raman or a direct THz interaction. In case of a Raman interaction, two non-resonant field interactions with a near IR pulse are needed. 2D-Raman spectroscopy requires three such Raman processes (two excitations and one read-out), hence it is a

---
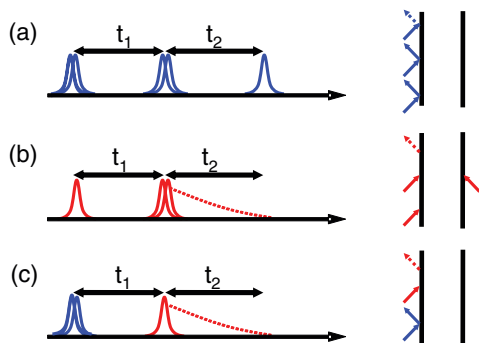
a)Electronic mail: phamm@pci.uzh.ch.

FIG. 1. Pulse sequences and a selection of possible double-sided Feynman diagrams in (a) 2D-Raman spectroscopy, in (b) 2D-THz spectrosocpy, and in (c) the hybrid 2D-Raman-THz spectroscopy discussed here. Blue pulses and arrows depict Raman interactions, the red ones THz interactions. The number of pulses in the left panels depicts the number of needed field interactions. If it is two field interactions at the same time, they may or may not originate from the same laser pulse in a concrete experimental implementation.

5th-order technique in which five incident field interactions interrogate the molecular system and trigger a field to be emitted (Fig. 1(a)). The high order of the process turned out to be the source of the problems of this method since there are several other competing processes, such as cascading, that are very difficult to separate experimentally.

Going down in Fig. 1, one sees that each Raman process with two field interactions with a non-resonant laser pulse can be replaced by a single field interaction with a low-frequency pulse that is resonant directly with the desired intermolecular modes of the liquid. Applying this rule literally, then 2D-THz spectroscopy would perturb the system with two THz fields, as such would be the 2nd-order nonlinearity, which, however, vanishes in an isotropic medium. Therefore, the experimental implementation of Refs. 42–44 was designed such that two field interactions are taken simultaneously from the second laser pulse (Fig. 1(b)). If one were to extract the two latter field interactions from two separate laser pulses, then this experiment would include a third time period, in which the system would evolve in a population state. Hence, conceptually speaking, 2D-THz spectroscopy directly in the low frequency regime is identical to conventional 2D-IR spectroscopy.[47]

On the other hand, if replacing only two of the Raman processes in 2D-Raman spectroscopy by a direct THz field interaction (Fig. 1(c)), the process is 3rd-order and as such allowed in isotropic media. This hybrid method will be referred to as 2D-Raman-THz spectroscopy. A near IR pulse generates a vibrational coherence by a Raman transition at time 0, which is then transferred into another coherence by a direct THz pulse at time t_1, that is finally read out by emitting a 3rd-order polarisation at time $t_1 + t_2$, again in the THz regime. Because it is 3rd-order, and because the two incident laser pulses have completely different frequencies, there are no issues with cascading. Furthermore, despite the fact that the 1D Raman response of water is weak, it can be measured with many orders of magnitudes signal-to-noise ratio.[12] As compared to 1D Raman spectroscopy, which is 3rd-order as well, the weak Raman read-out is replaced by a strong THz interaction in 2D-Raman-THz spectroscopy. The 2D-Raman-
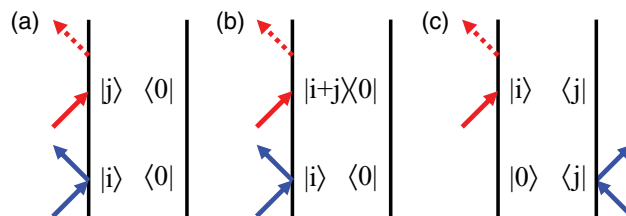

FIG. 2. The possible set of Feynman diagrams that occur in 2D-Raman-THz spectroscopy. Blue arrows depict the Raman interaction, red arrows the THz interactions. The labels use a harmonic picture as zero-order basis, in which $|i\rangle$ and $|j\rangle$ refer to a single quantum (fundamental) of modes i and j, respectively, and $|i + j\rangle$ to an combination mode if $i \neq j$, or an overtone if $i = j$. This selection of diagrams assume that one starts from the ground state $|0\rangle\langle 0|$, i.e., implicitly assumes zero temperature. For each thermally excited mode k, an equivalent set of diagrams exists, starting from a population state $|k\rangle\langle k|$.

THz spectrum therefore should be experimentally accessible as well.

Figure 2 shows the possible Feynman diagrams that occur in 2D-Raman-THz spectroscopy. Similar to 2D-Raman spectroscopy, each of these diagrams contains at least one two-quantum transition. That is, the incident or the emitted THz fields in diagrams (Figs. 2(a) and 2(c)), respectively, switch the *ket* of the density matrix from $|i\rangle$ to $|j\rangle$, i.e., effectively de-excites $|i\rangle$ and at the same time excite $|j\rangle$. Figure 2(b), on the other hand, emits from a combination mode $|i + j\rangle$ into the ground state. In the harmonic limit, two-quantum transitions would be forbidden. Hence, 2D-Raman-THz spectroscopy is specifically designed to detect the anharmonicity of the modes on the one hand (mechanical anharmonicity) and the anharmonicity of the dipole moment or the polarisibilty in dependence of the nuclear coordinates on the other hand.[23,25,26] The mechanical anharmonicity of intermolecular modes of liquids is expected to be significant. That is, the very fact that water is a liquid at room temperature with $k_B T = 200$ cm^{-1} shows that typical barriers in the high-dimensional intermolecular potential energy surface are of the same order of magnitude or smaller. Otherwise, water would be a glass at room temperature. When performing spectroscopy on intermolecular degrees of freedom, one is probing transitions in exactly the basins of this rugged energy landscape. With one vibrational quantum of such a transition in the 200 cm^{-1} regime, one would already reach the energy of the next barrier, so the harmonic picture becomes inadequate. Hence, it is not expected that the fact that 2D-Raman-THz spectroscopy relies on two-quantum transitions diminishes the size of the response very much. Quite the contrary, this discussion emphasizes that one has to give up thinking about vibrational spectroscopy in the low frequency range in terms of harmonic modes with a little bit of anharmonicity that can be treated perturbatively. A new language of the spectroscopy in this frequency range is yet to be developed.

II. THEORY

A. Response function

Conceptually speaking, 2D-Raman-THz spectroscopy is very similar to 2D-Raman spectroscopy. 2D-Raman spectroscopy is based on the following nonlinear response

function:[23]

$$R^{(5)}(t_2, t_1) = \left(\frac{i}{\hbar}\right)^2 \mathrm{Tr}(\mathbf{\Pi}(t_2 + t_1) \cdot [\mathbf{\Pi}(t_1), [\mathbf{\Pi}(0), \rho_{eq}]]),$$

(1)

where $[.., ..]$ is a commutator, $\Pi(t)$ the polarisibility operator at time t, and ρ_{eq} the equilibrium density matrix. In a 2D-Raman-THz experiment, the polarisibility operators at times t_1 and $t_1 + t_2$ are replaced by the corresponding dipole operators $\boldsymbol{\mu}(t_1)$ and $\boldsymbol{\mu}(t_1 + t_2)$:[45]

$$R^{(3)}(t_2, t_1) = \left(\frac{i}{\hbar}\right)^2 \mathrm{Tr}(\boldsymbol{\mu}(t_2 + t_1) \cdot [\boldsymbol{\mu}(t_1), [\mathbf{\Pi}(0), \rho_{eq}]]).$$

(2)

Due to the formal equivalence of both response functions, the theoretical treatment is very similar. The following calculation of the 2D-Raman-THz response is done in close analogy to Ref. 33.

In a first step, the expression is rewritten in the following form:

$$R^{(3)}(t_2, t_1) = \left(\frac{i}{\hbar}\right)^2 \mathrm{Tr}([\boldsymbol{\mu}(t_2 + t_1), \boldsymbol{\mu}(t_1)] \cdot [\mathbf{\Pi}(0), \rho_{eq}]),$$

(3)

which can be seen when multiplying out the commutators and making use of the invariance of the trace under cyclic permutation. In the classical limit, this translates into[48]

$$R^{(3)}(t_2, t_1) = \frac{1}{k_B T} \langle \{\boldsymbol{\mu}(t_2 + t_1), \boldsymbol{\mu}(t_1)\} \dot{\mathbf{\Pi}}(0) \rangle,$$

(4)

where $\{.., ..\}$ is the Poisson bracket, and where the following relationship has been used:[48]

$$\{\mathbf{\Pi}(0), \rho_{eq}\} = \dot{\mathbf{\Pi}}(0) \rho_{eq}/k_B T.$$

(5)

By shifting time zero, one gets

$$R^{(3)}(t_2, t_1) = \frac{1}{k_B T} \langle \{\boldsymbol{\mu}(t_2), \boldsymbol{\mu}(0)\} \dot{\mathbf{\Pi}}(-t_1) \rangle.$$

(6)

The direct evaluation of the Poisson bracket is numerically extremely tedious because it requires the calculation of the stability matrix.[49,50] In order to reduce the high demand of computer power, Tanimura and co-workers introduced a method which they termed the equilibrium-non-equilibrium hybrid approach.[33] That is, they run an equilibrium molecular dynamics (MD) trajectory from time $-t_1$ to time 0, explicitly perturb the trajectory at time 0 according to the interaction of the second laser pulse with the system, and then time-propagate this non-equilibrium trajectory until time t_2. (In the original "full" nonequilibrium approach, both the first and second interactions with laser pulses at times $-t_1$ and 0 are treated by introducing non-equilibrium perturbations, hence the simulations have to be repeated many times for varying times t_1.[28,31]) Furthermore, in order to suppress higher order nonlinear responses, two non-equilibrium trajectories perturbed by plus/minus the field of the second laser pulse are time-propagated, and the difference response is taken as the

final result

$$R^{(3)}(t_2, t_1) = \frac{1}{k_B T} \langle (\boldsymbol{\mu}_+(t_2) - \boldsymbol{\mu}_-(t_2)) \dot{\mathbf{\Pi}}(-t_1) \rangle_{nonequ.}$$

(7)

Here, the average is taken over an ensemble of non-equilibrium trajectories, and $\boldsymbol{\mu}_+(t_2)$ and $\boldsymbol{\mu}_-(t_2)$ refer to the dipole moments at time t_2 obtained after perturbing the momenta by $\pm \Delta p_i$, respectively, at time $t = 0$ (see Eq. (19) below).

B. Molecular model

The total polarisibility $\mathbf{\Pi}(t)$ of a MD simulation box is calculated as the sum of the polarisibilities of the individual water molecules $\boldsymbol{\alpha}_i(t)$ in the laboratory frame (whose time-dependence enters through the time dependent orientation of the molecule) plus the first order dipole-induced-dipole mechanism[51]

$$\mathbf{\Pi}(t) = \sum_{i=1}^{N/3} \boldsymbol{\alpha}_i + \sum_{i \neq j}^{N/3} \boldsymbol{\alpha}_i \mathbf{T}_{ij} \boldsymbol{\alpha}_j,$$

(8)

where $\mathbf{T}_{ij}$ is the dipole-dipole interaction tensor

$$\mathbf{T}_{ij} = \frac{1}{r_{ij}^5} \left(3 \mathbf{r}_{ij} \otimes \mathbf{r}_{ij} - r_{ij}^2 \mathbf{I}\right).$$

(9)

Here, $\mathbf{r}_{ij}$ is the vector connecting waters i and j (the center of mass of the water molecules is used as reference points), $\mathbf{I}$ the identity matrix, and $\otimes$ an outer product. We use the polarisibility $\boldsymbol{\alpha}_i$ introduced by Huiszoon[52] (in units of Å³)

$$\mathbf{\Pi} = \begin{pmatrix} 1.626 & 0 & 0 \\ 0 & 1.495 & 0 \\ 0 & 0 & 1.286 \end{pmatrix},$$

(10)

where the x-axis is defined as the axis connecting both hydrogens in the molecular frame, the y-axis the dipole axis, and the z-axis, the axis perpendicular to the molecular plain. The 1D Raman response $\langle \mathbf{\Pi}(t) \dot{\mathbf{\Pi}}(0) \rangle$ agrees perfectly with the one shown in Ref. 29 (compare Fig. 3(a) with the solid line in Fig. 2 of that reference). Also shown is the corresponding Raman spectrum, defined as

$$I_{\mathrm{Raman}}(\omega) \propto \frac{1 - e^{-\beta \hbar \omega}}{(\omega - \omega_L)^4} \Im \int_0^\infty e^{i\omega t} \langle \mathbf{\Pi}(t) \dot{\mathbf{\Pi}}(0) \rangle dt, \quad (11)$$

where ω_L is the exciting laser frequency. Similar to the experimental Raman spectrum,[13,53] three spectral features can be identified: a dominating band at about ≈ 200 cm⁻¹, which is commonly assigned to the hydrogen bond stretch vibration, a shoulder at ≈ 60 cm⁻¹ (a hydrogen bond bend vibration), and a broad decaying slope that extends from ≈ 400 cm⁻¹ to beyond ≈ 1000 cm⁻¹ (hindered rotation or libration). Since a rigid water model (SPC/E water) is used in the simulation (see below), only the intermolecular degrees of freedom show up in the spectrum.
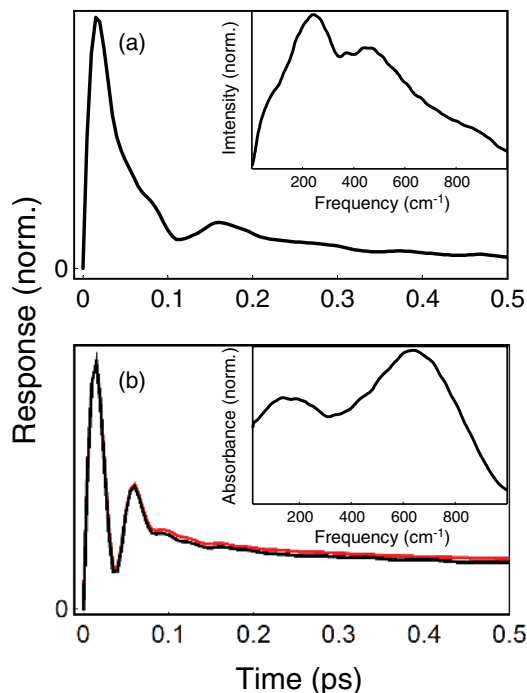
FIG. 3. (a) 1D Raman response $\langle \mathbf{\Pi}(t)\dot{\mathbf{\Pi}}(0)\rangle$ and (b) 1D THz response $\langle \boldsymbol{\mu}(t)\dot{\boldsymbol{\mu}}(0)\rangle_{equ}$ calculated from a 10 ns equilibrium trajectory. In panel (b), the line in red originates from the properly scaled nonequilibrium response $\langle \boldsymbol{\mu}_{+}(t_2) - \boldsymbol{\mu}_{-}(t_2)\rangle_{nonequ}$, which is slightly offset for better visibility. The insets show the corresponding spectra according to Eqs. (11) and (17), respectively

The analogous approach to describe the total dipole moment would be

$$\boldsymbol{\mu}(t) = \sum_{i=1}^{N/3} \boldsymbol{\mu}_i + \sum_{i \neq j}^{N/3} \boldsymbol{\alpha}_i \boldsymbol{T}_{ij} \boldsymbol{\mu}_j, \quad (12)$$

where $\boldsymbol{\mu}_i$ is the non-polarisable dipole moment of water i, which can be calculated from the point charges of the MD model. The second term accounts for the dipole-induced dipole effect. It has been shown that this second term reproduces the 200 cm^{-1} band of water,[54] however, severely underestimates its intensity (the first term does not capture this band at all). It is well established that the intensity of this band is the result of intra- and intermolecular charge flows upon hydrogen bonding, which requires explicit quantum-chemistry calculations to correctly describe them.[18–21] Since the 200 cm^{-1} band will be the major target of our experiment, the approach of Ref. 18 is followed instead of Eq. (12) for a computationally inexpensive parameterization of these charge flow effects (despite a slightly different language, Torii[21] uses the same approach with a similar parameterization). That is, a "dynamical charge" is assigned to each hydrogen and oxygen atom, which is defined as the change of total dipole moment induced by a displacement of its nuclear coordinates

$$Z_{ij} = \frac{\partial \mu_i}{\partial q_j}, \quad (13)$$

where the indices i and j label the $\{x, y, z\}$ coordinates. If the source of the dipole of a molecule were just the static point charges localized at each atom, as they are in a non-

polarizable MD force field, then Eq. (13) would be a scalar (i.e., a diagonal matrix with all identical diagonal elements) and would reveal exactly these point charges. In general, however, the dynamical charge Z_{ij} is a (3×3)-tensor in order to account for the fact that the charge flow is anisotropic and furthermore not necessarily parallel to the displacement of atoms.

With this definition, it is straightforward to calculate the time-derivative of the dipole moment

$$\dot{\mu}_i(t) = \sum_{j=\{x,y,z\}} Z_{ij} v_j, \quad (14)$$

where v_j is the velocity of the atom that is readily obtained from a MD simulation. In contrast to Refs. 18 and 21, the motion of the individual atoms is not transformed into a center of mass translation and a rotation of each water molecule as a whole. The third order response function Eq. (7), as well as the linear response function $\langle \boldsymbol{\mu}(t)\dot{\boldsymbol{\mu}}(0)\rangle$, requires the calculation of $\boldsymbol{\mu}(t)$ instead of its time-derivative, which is performed by numerical integration. Since this integration accumulates numerical errors, it does not exactly reproduce the correct long time limit $\langle \boldsymbol{\mu}(t)\dot{\boldsymbol{\mu}}(0)\rangle \to 0$ for $t \to \infty$, but this is not a problem for the short time periods of ≤ 1.5 ps considered here. The dipole correlation function is expected to decay on a 10 ps timescale, which has been verified when employing the direct dipole moment definition (Eq. (12)).

In principle, the dynamical charges of a given water molecule depend on its detailed environment. However, it has been shown in Refs. 18 and 21 that a reasonable agreement with the experimental THz spectrum is obtained when using identical dynamical charges for all water molecules. The averaged dynamical charges were calculated in Ref. 18 from an *ab initio* MD simulation of a small water box and are used here after symmetrizing them

$$Z_{\mathrm{O}} = \begin{pmatrix} -1.15 & 0 & 0 \\ 0 & -0.99 & 0 \\ 0 & 0 & -1.08 \end{pmatrix}, \quad (15)$$

$$Z_{\mathrm{H}} = \begin{pmatrix} 0.80 & 0.31 & 0 \\ 0.31 & 0.45 & 0 \\ 0 & 0 & 0.35 \end{pmatrix} \quad (16)$$

with the same definition of the molecular frame as for Eq. (10). Figure 3(b), black line, shows the resulting 1D response function, $\langle \boldsymbol{\mu}(t)\dot{\boldsymbol{\mu}}(0)\rangle$, as well as the THz absorption spectrum calculated as

$$I_{\mathrm{THz}}(\omega) \propto \left(1 - e^{-\beta\hbar\omega}\right) \Im \int_0^\infty e^{i\omega t} \langle \boldsymbol{\mu}(t)\dot{\boldsymbol{\mu}}(0)\rangle dt, \quad (17)$$

which agrees reasonably well with the experimental THz spectrum.[55] The dominating band is the hindered rotation (libration motion) peaking at ≈ 600 cm^{-1} in the THz spectrum (the corresponding intensity is weaker in the Raman spectrum since the polarisability of the water molecule is quite isotropic). As anticipated, the 200 cm^{-1} band is reproduced realistically.

Another way to think about the dynamical charges is in terms of the force an external field exerts on an atom

$$F_i = \sum_{j=\{x,y,z\}} Z_{ij} E_j. \tag{18}$$

This expression allows one to calculate the non-equilibrium perturbation of the THz pulse at time 0 needed to calculate Eq. (7). An impulsive limit is assumed, i.e., the momenta of all atoms are changed due to the force generated by a quasi δ-shaped THz pulse of length Δt:

$$\Delta p_i = F_i \Delta t = \sum_{j=\{x,y,z\}} Z_{ij} E_j \Delta t. \tag{19}$$

As a consistency check, it has been verified that the 1D THz response $\langle \boldsymbol{\mu}_+(t_2) - \boldsymbol{\mu}_-(t_2) \rangle_{nonequ}$ calculated with the non-equilibrium method (i.e., defined in analogy to Eq. (7), see Fig. 3(b), red line) agrees with the equilibrium correlation function, $\langle \boldsymbol{\mu}(t_2)\dot{\boldsymbol{\mu}}(0) \rangle_{equ}$ (Fig. 3(b), black line) calculated from a 10 ns equilibrium trajectory. This comparison also allows one to adjust the integrated pulse field $\boldsymbol{E}\Delta t$ such that one stays in a linear regime.

C. MD details

MD simulations of rigid SPC/E water were performed with the GROMACS program package.[56] Sixty four water molecules were simulated in a box of size 1.2446 nm with periodic boundary conditions, with 2.5 fs time-step, with a cut-off of the Lennard-Jones interactions at 0.6 nm (switched to zero at 0.5 nm), and with the long-range electrostatic forces approximated by the Particle-Mesh-Ewald approximation. The velocity Verlet integration was chosen instead of leapfrog integration, since the former outputs velocities and positions at the same time points, both of which are needed for the calculation of Eq. (14). A Berendsen thermostat at 300 K was applied (i.e., a NVT ensemble), albeit with a long coupling time of 5 ps in order to perturb the non-equilibrium trajectories not too much. By calculating also the 1D Raman response of 128 water molecules in a correspondingly larger box with larger cut-offs, it has been verified that the results are not affected by the small number of water molecules.

To evaluate Eq. (7), a equilibrium trajectory was calculated in consecutive pieces of 1.5 ps. At the end-point of each of these pieces, the momenta were perturbed by $\pm \Delta p_i$ according to Eq. (19), and two non-equilibrium trajectories were propagated for 1.5 ps each. For the value chosen for the integrated pulse field, $\boldsymbol{E}\Delta t$, the average kinetic energy (i.e., the temperature) changed by about 50% after perturbing the momenta. Together with the equilibrium trajectory, the two corresponding non-equilibrium trajectories revealed one sample of the average Eq. (7) for all times t_1 and t_2 on a grid of step size 5 fs with $0 < t_{1,2} < 1.5$ ps (only 0.5 ps are shown in Fig. 4). Equation (7) was averaged over $\approx 5.6 \times 10^7$ such samples, amounting to a total simulation time of ≈ 250 μs. The simulation took about six weeks on a workstation with 48 cores running at 2.3 GHz.

III. RESULTS AND DISCUSSION

Figure 4(a) shows the simulated 2D-Raman-THz response $R_{xxxx}^{(3)}(t_1, t_2)$ in the time-domain with Raman-pump and THz pulse polarized in parallel. Along both axes, the 2D response resembles to a certain extent the corresponding 1D responses (Fig. 3). For example, the ridge for long times is larger and longer lived for the THz (t_2) axis than for the Raman (t_1) axis (see label (1) versus label (2)), and their oscillatory components are similar as well. It is, however, important to stress that the 2D-Raman-THz response is not just a simple product of the 1D responses

$$R_{xxxx}^{(3)}(t_1, t_2) \neq R_{\text{Raman}}^{(1)}(t_1) \cdot R_{\text{THz}}^{(1)}(t_2), \tag{20}$$

which can be seen for example from the two negative (blue) dips marked as label (3) in the 2D-Raman-THz response (Fig. 4(a)), while neither of the 1D response functions is ever negative. Hence, clearly both time coordinates are correlated, and as such the 2D response contains additional information about coupling and correlations between degrees of freedom beyond the 1D THz and Raman responses. Nevertheless, no ridge along the diagonal is observed, indicating that no echo is generated. The 2D-Raman-THz signal looks quite different from 2D-Raman signals calculated in literature,[24,29,33] presumably since the THz pulse is selective to different modes.

The perpendicular signal $R_{xxyy}^{(3)}$ has opposite sign but apart from that, features a very similar response (Fig. 4(b)). The initial peak near $t_1 = t_2 = 0$ in the perpendicular signal is about 46% of the size of that in the parallel signal. The remaining possible polarization conditions are $R_{xyxy}^{(3)}$ and $R_{yxxy}^{(3)}$. Both would be measured simultaneously since the Raman-pump process is instantaneous and one has no control over the time ordering of first and second field interaction. Furthermore, the four possible polarization conditions are linearly dependent[47]

$$R_{xyxy}^{(3)} + R_{yxxy}^{(3)} = R_{xxxx}^{(3)} - R_{xxyy}^{(3)}. \tag{21}$$

Given the very similar shape of $R_{xxxx}^{(3)}$ and $R_{xxyy}^{(3)}$, also $R_{xyxy}^{(3)} + R_{yxxy}^{(3)}$ looks essentially the same and therefore is not shown in Fig. 4.

In conventional 2D-IR spectroscopy, it became common to transform coherence time periods into the frequency domain by a 2D Fourier transformation.[47] Principally speaking, the only reason for doing this is to obtain a more intuitive presentation of data, as the physical information content of a time- or a frequency-domain representation is, of course, the same. Although the 2D-Raman literature usually presents the response in the time-domain (with the exception of Ref. 29), a frequency domain representation is favored here because the low-frequency spectra of water still show some structure that can be assigned to certain modes, so a cross peak in a 2D spectrum hints to a coupling between degrees of freedom, etc. It should be stressed though that the set of Feynman diagrams giving rise to 2D-Raman-THz spectroscopy (Fig. 2) is different from 2D-IR spectroscopy. Consequently, the language used for the interpretation of 2D-IR spectra cannot necessarily be transferred to 2D-Raman-THz spectroscopy (or 2D-Raman spectroscopy) in a one-to-one manner. Many more model studies will be needed to learn how to read these
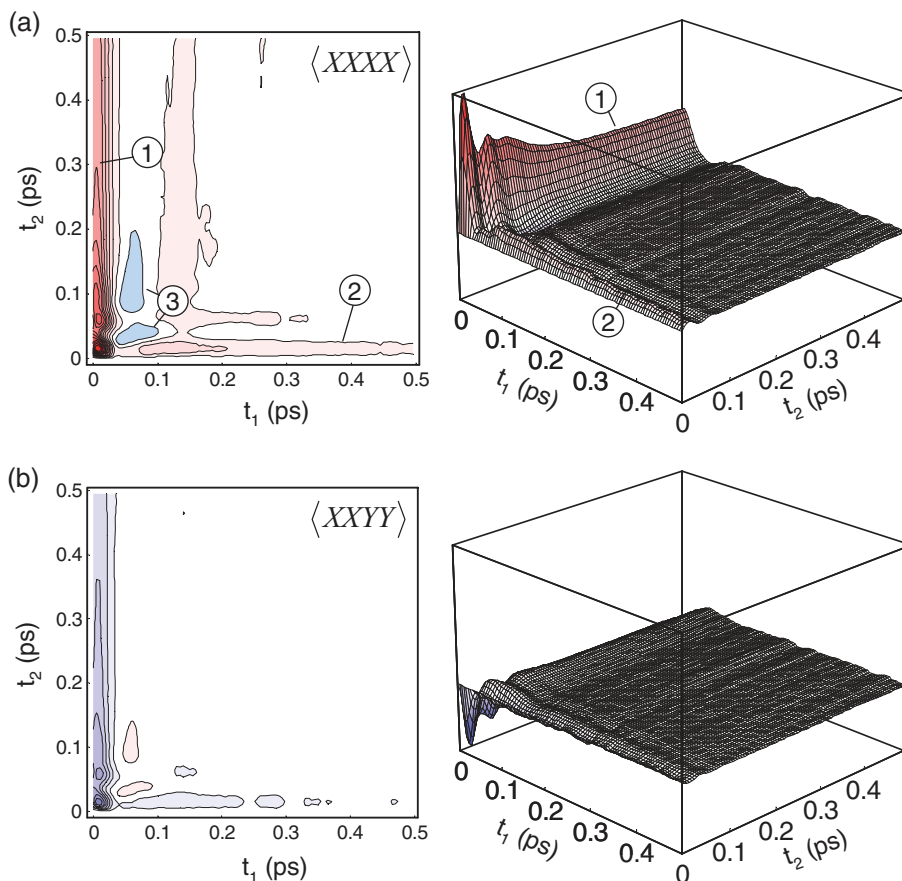
FIG. 4. Simulated 2D-Raman-THz response in the time-domain with (a) $\langle XXXX \rangle$ polarisation condition (Raman-pump and THz pulse polarized in parallel) and (b) $\langle XXYY \rangle$ polarisation condition (Raman-pump and THz pulse perpendicular). In both cases, the responses are shown as contour plots (left) as well as in a 3D representation (right). Both signals are scaled the same way so their signal sizes can be compared. Red and blue colors indicate positive and negative signs, respectively, of the response function (the i^2 factor of Eq. (2) is not included in the presentation, which will flip the sign of the response function). The labels refer to features discussed in the text.

spectra, and the discussion below is considered to be an attempt in this direction. Ultimately, the aim of such a discussion is to put the black-box simulation from the previous paragraph into physical terms.

The first difference is encountered when trying to plot purely absorptive 2D spectra. Purely absorptive 2D spectra are desired since they reveal the highest spectral resolution and the most intuitive representation of the data.[57] In 2D-IR spectroscopy, purely absorptive spectra are obtained by measuring both non-rephasing and rephasing diagrams and adding them up in a proper way.[47] The same is not possible in 2D-Raman-THz spectroscopy. Non-rephasing (Figs. 2(a) and 2(b)) and rephasing (Fig. 2(c)) diagrams do indeed exist, in the sense that the latter switches the order of the coherence from the *bra* to the *ket* of the density matrix (assuming $\omega_i > \omega_j$), while the former does not. Furthermore, as long as one does not make use of any phase matching or phase cycling, both rephasing and non-rephasing diagrams are indeed measured simultaneously, like in a pump-probe configuration of 2D-IR spectroscopy.[58–60] However, unlike in 2D-IR spectroscopy, both sets of diagrams are not symmetric in 2D-Raman-THz spectroscopy. That is, the non-rephasing diagram emits at frequency ω_j and $\omega_j + \omega_i$ (Figs. 2(a) and 2(b)), respectively, while the corresponding rephasing diagram emits at frequency $\omega_i - \omega_j$ (Fig. 2(c)), so the phase twist of the

two contributions would not cancel. As discussed in the Appendix, purely absorptive spectra can still be obtained by a 2D sine-Fourier transformation (see Fig. 5)

$$R(\omega_1, \omega_2) = a(\omega_1, \omega_2)$$
$$\cdot \int_0^\infty \int_0^\infty R(t_1, t_2) \sin(\omega_1 t_1) \sin(\omega_2 t_2) dt_1 dt_2,$$
(22)

where $a(\omega_1, \omega_2)$ is the product of the two frequency prefactors as in Eqs. (11) and (17). These prefactors are quantum-correction factors that are correct only in the harmonic case.

While the harmonic approximation might still be reasonable for the linear case (Eqs. (11) and (17)), 2D-Raman-THz spectroscopy is exclusively sensitive to the anharmonic contribution (see discussion in Sec. I). On the other hand, while, e.g., the absorption cross section $I_{THz}(\omega)$ is a rigorously defined experimental observable, a 2D spectrum (Eq. (22)) is just used for a more intuitive graphical representation of the response function. We may therefore use the same prefactors to facilitate a better comparison with the 1D spectra in Fig. 3, despite the fact that the harmonic approximation is certainly not adequate for the 2D response.

The first immediate observation is that the 2D-Raman-THz spectrum is exclusively positive, unlike a 2D-IR
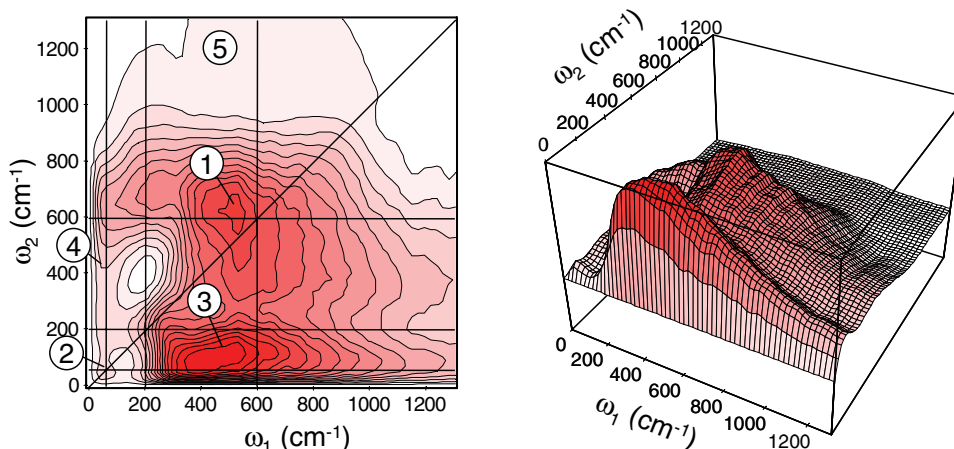
FIG. 5. 2D-Raman-THz response of the $\langle XXXX \rangle$ response in the frequency domain. The responses is shown as contour plots (left) as well as in a 3D representation (right). Red and blue colors indicate positive and negative signs, respectively, of the response function. The grid in panel (b) guides the eye to the positions where the major spectral features showing up in the 1D and 1D THz spectra at 60 cm^{-1} (hydrogen bond bending), 200 cm^{-1} (hydrogen bond stretching) and 600 cm^{-1} (libration). The labels refer to features discussed in the text.

spectrum. Note that this is *not* an artefact of the sine-Fourier transformation and that this is *not* an absolute value spectrum. In conventional 2D-IR spectroscopy, bleach and stimulated emission contributions have opposite sign as compared to the excited state absorption. On the contrary, the Feynman diagrams shown in Fig. 2 involve only coherences but never populate an excited state, as such no processes that could be classified as excited state absorption versus stimulated emission can be identified, both of which would have opposite signs.

Along the diagonal of the 2D spectrum (Fig. 5), signals related to the 600 cm^{-1} band (hindered rotation or libration) and the 60 cm^{-1} band (hydrogen-bond bending) lead to distinct peaks marked as labels (1) and (2), respectively. In contrast, the 200 cm^{-1} band hardly shows up along the diagonal. Neither of these the diagonal peaks is tilted in the 2D spectrum, so one would conclude that the lines are not inhomogeneously broadened. The 600 cm^{-1} band is somewhat off the diagonal, which can be understood from the 1D responses in Fig. 3, where the corresponding band peaks at about 450 cm^{-1} in the Raman spectrum and at about 600 cm^{-1} in the THz spectrum. This so-called non-coincident effect[61] hints towards an excitonic delocalization, in which case the different selection rules of Raman and THz interactions bring out different energy regions of the excitonic band. As the most simple example of the non-coincident effect, consider the normal modes of CO_2, whose symmetric combination of the C=O stretch vibrations is Raman active and lower in frequency, while the antisymmetric combination is IR active and higher in frequency.

In addition, two broad cross-peak features show up in the 2D spectrum labeled as Eqs. (3) and (4). Feature (3) relates to the librational mode along the Raman (ω_1) axis, but does not resolve the 60 cm^{-1} from the 200 cm^{-1} mode along the THz (ω_2) axis, just like the 1D THz spectrum does not resolve these two bands (Fig. 3). The tilt of the crosspeak, however, suggests that the lower frequency part of the Raman response couples more to the 60 cm^{-1} mode and the higher frequency part more to the 200 cm^{-1} mode. The opposite cross peak (label 4), in contrast, is clearly mostly due to a coupling between

the libration mode and the hydrogen bond bending mode at 60 cm^{-1}. This makes sense since both involve rotational motions of the water molecules, whereas the hydrogen stretch vibration at 200 cm^{-1} is expected to decouple from the two.

From the Feynman diagram (Fig. 2(b)), one might expect that light at frequencies related to combination modes and overtones is emitted along the THz frequency ω_2. There is a weak shoulder labeled (5) in Fig. 5, which could be assigned to such an overtone of the libration mode (i.e., 450 cm^{-1} for the Raman frequency ω_1 and $\approx 2 \times 600 = 1200$ cm^{-1} for the THz frequency ω_2), but its intensity is very weak. In essence, one may conclude from the lack of clear overtones that the harmonic approximation, which is at the background of the labeling of the Feynman diagrams of Fig. 2, is not valid. That is, if one were to redefine i and j to label eigenstates rather than fundamentals of normal modes, then Feynman diagram Fig. 2(b) would become obsolete since there is no such thing as the combination of two eigenstates $i + j$, i.e., it would just be another eigenstate j which is already captured by the Feynman diagram in Fig. 2(a). In other words, if one completely looses selection rules and two-quantum transitions become equally allowed as one-quantum transitions (where the very word "two-quantum transition" resorts to a harmonic picture), then the 1D spectrum reflects the density of eigenstates instead of the density of fundamentals of normal modes, and the same will be true for any spectral feature in the 2D-Raman-THz spectrum. Hence, one does not expect much intensity in the 2D-Raman-THz spectrum outside the region where there is intensity in the corresponding 1D spectra, as is observed in Fig. 5. The lack of overtone emission, as depicted by Feynman diagram in Fig. 2(b), also evidences that the signal size of the 2D-Raman-THz spectroscopy is not limited by the fact that the signal relies on two-quantum transitions.

IV. CONCLUSION

In this paper, a new 2D spectroscopy, 2D-Raman-THz spectroscopy, is discussed. The information content of 2D-Raman-THz spectroscopy is similar to 2D-Raman or 2D-THz

spectroscopy, but it circumvents the major problems of these techniques, and hence should be realizable experimentally. Using water as an interesting test case, the 2D-Raman-THz has been simulated from an all-atom MD simulation, and the potential information content of the expected 2D spectra is discussed. As the intermolecular Raman and THz spectrum measures the motion of water molecules directly, the corresponding experimental spectrum, once it becomes available, will serve as the most stringent test to date of water computer models. Furthermore, the extension of the technique to solvation water around ions, hydrophobes, or proteins, all of which having a large effect on the intermolecular spectrum of water,[15–17] appears to be extremely promising. When comparing the simulations with experimental results, one must of course bear in mind that Eq. (2) is a response function, hence assume a δ-shaped THz pulse, which, however, does not exist in reality. The closest approximation to a δ-pulse is a "single-cycle" THz pulse, which ideally takes the form of the second derivative of the envelope of an ultrashort generating pulse in an optical rectification process. The measured signal will be a convolution of the response function with that 2nd derivative pulse.

Cho has discussed various variants of 2D spectroscopy, interchanging the time-ordering of the THz and Raman interactions.[45] In an experimental realization, the THz-Raman-THz sequence, which will contain complementary information, will automatically be measured in different quadrants of a (t_1, t_2) plot, while the THz-THz-Raman sequence would require a completely different experimental design, because the read-out is the Raman process.

We are currently working on an experimental implementation of 2D-Raman-THz spectroscopy in our lab. Preliminary results reveal an emitted THz field that is $\approx 10^{-4}$ of the incident THz field for a Raman pump energy that is below the threshold of higher order processes such as multi-photon ionization of water. Similar to 2D-Raman spectroscopy, the simulation presented here will serve as a guide to search for and to verify the small experimental signal.

ACKNOWLEDGMENTS

APPENDIX: PURELY ABSORPTIVE LINESHAPES IN 2D-RAMAN-THz SPECTROSCOPY

By a simple trick, one may obtain purely absorptive spectra of the 2D-Raman-THz response despite the fact that no symmetric set of rephasing and non-rephasing Feynman diagrams exists. That is, rather than taking a complex 2D Fourier transformation of the time-domain response function:

$$R(\omega_1, \omega_2) = \Im \int_0^\infty \int_0^\infty R(t_1, t_2) e^{i\omega_1 t_1} e^{i\omega_2 t_2} dt_1 dt_2, \quad (A1)$$
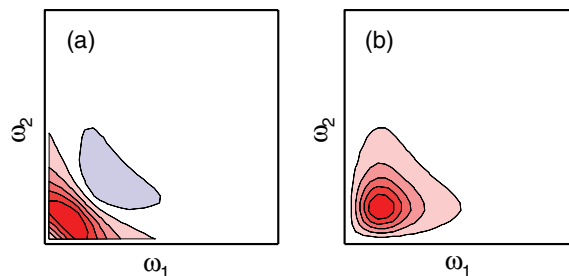

FIG. 6. 2D spectrum of a strongly damped vibrator (i.e., Eq. (A5) with $\gamma = \omega$) calculated (a) with a complex 2D Fourier transformation Eq. (A1) and (b) a 2D sine-Fourier transformation Eq. (A1).

one should take a sine-Fourier transformation:

$$R(\omega_1, \omega_2) = \int_0^\infty \int_0^\infty R(t_1, t_2) \sin(\omega_1 t_1) \sin(\omega_2 t_2) dt_1 dt_2. \quad (A2)$$

To see why this is the case, consider as an example the following 1D response function:

$$R(t_1) \propto \sin(\omega t_1) e^{-\gamma(t_1)}, \quad (A3)$$

whose 1D Fourier-transformation contains absorptive $A(\omega_1)$ and dispersive $D(\omega_1)$ contributions:

$$\int_0^\infty R(t_1) e^{i\omega_1 t_1} dt_2 = D(\omega_1) + i A(\omega_1). \quad (A4)$$

Since the 1D response functions are odd functions (see Eqs. (11) and (17)), the imaginary part is absorptive. Now consider a 2D response function without correlation between both time-coordinates

$$R(t_1, t_2) \propto \sin(\omega t_1) \sin(\omega t_2) e^{-\gamma(t_1 + t_2)}. \quad (A5)$$

A complex Fourier transformation with Eq. (A1) intermixes dispersive and absorptive contributions

$$(D(\omega_1) + i A(\omega_1)) \cdot (D(\omega_2) + i A(\omega_2))$$
$$= D(\omega_1) D(\omega_2) - A(\omega_1) A(\omega_2)$$
$$+ i (D(\omega_1) A(\omega_2) + A(\omega_1) D(\omega_2)) \quad (A6)$$

whereas a sine-Fourier transformation Eq. (A2) reveals the desired $A(\omega_1) A(\omega_2)$. Figure 6 demonstrates the difference for a single strongly damped oscillator. The sine-Fourier transformation (Fig. 6(b)) reveals the much more intuitive representation of the spectrum.

[1]J. B. Asbury, T. Steinel, K. Kwak, S. A. Corcelli, C. P. Lawrence, J. L. Skinner, and M. Fayer, J. Chem. Phys. **121**, 12431 (2004).

[2]S. Yeremenko, M. S. Pshenichnikov, and D. A. Wiersma, Chem. Phys. Lett. **369**, 107 (2003).

[3]M. L. Cowan, B. D. Bruner, N. Huse, J. R. Dwyer, B. Chugh, E. T.J. Nibbering, T. Elsaesser, and R. J. D. Miller, Nature (London) **434**, 199 (2005).

[4]J. D. Eaves, J. J. Loparo, C. J. Fecko, S. T. Roberts, A. Tokmakoff, and P. L. Geissler, Proc. Natl. Acad. Sci. U.S.A. **102**, 13019 (2005).

[5]S. Garrett-Roe, F. Perakis, F. Rao, and P. Hamm, J. Phys. Chem. B **115**, 6976 (2011).

[6]F. Perakis and P. Hamm, J. Chem. Phys. B **115**, 5289 (2011).

[7]K. B. Moller, R. Rey, and J. T. Hynes, J. Phys. Chem. A **108**, 1275 (2004).

[8]C. J. Fecko, J. D. Eaves, J. J. Loparo, A. Tokmakoff, and P. L. Geissler, Science **301**, 1698 (2003).

[9]C. P. Lawrence and J. L. Skinner, J. Chem. Phys. **117**, 8847 (2002).

[10]J. D. Smith, C. D. Cappa, K. R. Wilson, R. C. Cohen, P. L. Geissler, and R. J. Saykally, Proc. Natl. Acad. Sci. U.S.A. **102**, 14171 (2005).

[11]S. Garrett-Roe and P. Hamm, Acc. Chem. Res. **42**, 1412 (2009).

[12]T. Torre, P. Bartolini, and R. Righini, Nature (London) **428**, 296 (2004).

[13]T. Fukasawa, T. Sato, J. Watanabe, Y. Hama, W. Kunz, and R. Buchner, Phys. Rev. Lett. **95**, 197802 (2005).

[14]N. T. Hunt, L. Kattner, R. P. Shanks, and K. Wynne, J. Am. Chem. Soc. **129**, 3168 (2007).

[15]I. A. Heisler and S. R. Meech, Science **327**, 857 (2010).

[16]K. Mazur, I. A. Heisler, and S. R. Meech, J. Phys. Chem. B **115**, 2563 (2011).

[17]S. Ebbinghaus, S. J. Kim, M. Heyden, X. Yu, U. Heugen, M. Gruebele, D. M. Leitner, and M. Havenith, Proc. Natl. Acad. Sci U.S.A. **104**, 20749 (2007).

[18]A. Pasquarello and R. Resta, Phys. Rev. B **68**, 174302 (2003).

[19]M. Sharma, R. Resta, and R. Car, Phys. Rev. Lett. **95**, 187401 (2005).

[20]M. Heyden, J. Sun, S. Funker, G. Mathies, H. Forbert, M. Havenith, and D. Marx, Proc. Natl. Acad. Sci. U.S.A. **107**, 12068 (2010).

[21]H. Torii, J. Phys. Chem. B **115**, 6636 (2011).

[22]R. F. Loring and S. Mukamel, J. Chem. Phys. **83**, 2116 (1985).

[23]Y. Tanimura and S. Mukamel, J. Chem. Phys. **99**, 9496 (1993).

[24]S. Palese, J. T. Buontempo, L. Schilling, W. T. Lotshaw, Y. Tanimura, S. Mukamel, and R. J. D. Miller, J. Chem. Phys. **98**, 12466 (1994).

[25]K. Okumura and Y. Tanimura, J. Chem. Phys. **106**, 1687 (1997).

[26]K. Okumura and Y. Tanimura, J. Chem. Phys. **107**, 2267 (1997).

[27]A. Man and R. M. Stratt, Phys. Rev. Lett. **85**, 1004 (2000).

[28]T. L. Jansen, J. G. Snijders, and K. Duppen, J. Chem. Phys. **113**, 307 (2000).

[29]S. Saito and I. Ohmine, J. Chem. Phys. **108**, 240 (1998).

[30]S. Saito and I. Ohmine, Phys. Rev. Lett. **88**, 207401 (2002).

[31]S. Saito and I. Ohmine, J. Chem. Phys. **119**, 9073 (2003).

[32]Y. Nagata and Y. Tanimura, J. Chem. Phys. **124**, 024508 (2006).

[33]T. Hasegawa and Y. Tanimura, J. Chem. Phys. **125**, 074512 (2006).

[34]T. Yagasaki and S. Saito, Acc. Chem. Res. **42**, 1250 (2009).

[35]A. Tokmakoff, M. J. Lang, D. S. Larsen, G. R. Fleming, V. Chernyak, and S. Mukamel, Phys. Rev. Lett. **79**, 2702 (1997).

[36]D. A. Blank, L. J. Kaufman, and G. R. Fleming, J. Chem. Phys. **111**, 3105 (1999).

[37]D. A. Blank, L. J. Kaufman, and G. R. Fleming, J. Chem. Phys. **113**, 771 (2000).

[38]L. J. Kaufman, J. Heo, L. D. Ziegler, and G. R. Fleming, Phys. Rev. Lett. **88**, 207402 (2002).

[39]K. J. Kubarych, C. J. Milne, and R. J. D. Miller, Int. Rev. Phys. Chem. **22**, 497 (2003).

[40]O. Golonzka, N. Demirdöven, M. Khalili, and A. Tokmakoff, J. Chem. Phys. **113**, 9893 (2000).

[41]Y. L. Li, L. Huang, R. J. D. Miller, T. Hasegawa, and Y. Tanimura, J. Chem. Phys. **128**, 234507 (2008).

[42]W. Kuehn, K. Reimann, M. Woerner, and T. Elsaesser, J. Chem. Phys. **130**, 164503 (2009).

[43]W. Kuehn, K. Reimann, M. Woerner, T. Elsaesser, and R. Hey, J. Phys. Chem. B **115**, 5448 (2011).

[44]W. Kuehn, K. Reimann, M. Woerner, T. Elsaesser, R. Hey, and U. Schade, Phys. Rev. Lett. **107**, 067401 (2011).

[45]M. Cho, J. Chem. Phys. **111**, 4140 (1999).

[46]R. R. Ernst, G. Bodenhausen, and A. Wokaun, *Principles of Nuclear Magnetic Resonance in One and Two Dimensions* (Clarendon, Oxford, 1987).

[47]P. Hamm and M. T. Zanni, *Concepts and Methods of 2D Infrared Spectroscopy* (Cambridge University Press, Cambridge, 2011).

[48]S. Mukamel, *Principles of Nonlinear Optical Spectroscopy* (Oxford University Press, Oxford, 1995).

[49]J. Jeon and M. Cho, New J. Phys. **12**, 065001 (2010).

[50]S. Mukamel, V. Khidekel, and V. Chernyak, Phys. Rev. E **53**, R1 (1995).

[51]J. Applequist, J. R. Carl, and K.-K. Fung, J. Am. Chem. Soc. **94**, 2952 (1972).

[52]C. Huiszoon, Mol. Phys. **58**, 865 (1986).

[53]S. Krishnamurthy, R. Bansil, and J. Wiafe-Akenten, J. Chem. Phys. **79**, 5863 (1983).

[54]P. A. Madden and R. W. Impey, Chem. Phys. Lett. **123**, 502 (1986).

[55]J. E. Bertie and Z. Lan, Appl. Spectroscopy **50**, 1047 (1996).

[56]D. van der Spoel, E. Lindahl, B. Hess, G. Groenhof, A. E. Mark, and H. J. C. Berendsen, J. Comput. Chem. **26**, 1701 (2005).

[57]M. Khalil, N. Demirdöven, and A. Tokmakoff, Phys. Rev. Lett. **90**, 047401 (2003).

[58]L. P. DeFlores, R. A. Nicodemus, and A. Tokmakoff, Opt. Lett. **32**, 2966 (2007).

[59]S. H. Shim and M. T. Zanni, Phys. Chem. Chem. Phys. **11**, 748 (2009).

[60]J. Helbing and P. Hamm, J. Opt. Soc. Am. B **28**, 171 (2011).

[61]H. Torii, Chem. Phys. Lett. **323**, 382 (2000).